

Spectral Phase Encoding for Quantum Kernel Methods

Pablo Herrero Gómez¹, Antonio Jimeno Morenilla¹, David Muñoz-Hernández¹, and Higinio Mora Mora¹

¹Department of Computer Science Technology and Computation,
University of Alicante, Alicante, Spain

Abstract

Quantum kernel methods are promising for near-term quantum machine learning, yet their behavior under data corruption remains insufficiently understood. We analyze how quantum feature constructions degrade under controlled additive noise.

We introduce *Spectral Phase Encoding* (SPE), a hybrid construction combining a discrete Fourier transform (DFT) front-end with a diagonal phase-only embedding aligned with the geometry of diagonal quantum maps. Within a unified framework, we compare QK-DFT against alternative quantum variants (QK-PCA, QK-RP) and classical SVM baselines under identical clean-data hyperparameter selection, quantifying robustness via dataset fixed-effects regression with wild cluster bootstrap inference across heterogeneous real-world datasets.

Across the quantum family, DFT-based preprocessing yields the smallest degradation rate as noise increases, with statistically supported slope differences relative to PCA and RP. Compared to classical baselines, QK-DFT shows degradation comparable to linear SVM and more stable than RBF SVM under matched tuning. Hardware experiments confirm that SPE remains executable and numerically stable for overlap estimation. These results indicate that robustness in quantum kernels depends critically on structure-aligned preprocessing and its interaction with diagonal embeddings, supporting a robustness-first perspective for NISQ-era quantum machine learning.

Keywords: quantum kernels, data encoding, spectral methods, robustness, NISQ computing

1 Introduction

Quantum machine learning (QML) has attracted considerable attention as a potential avenue for leveraging near-term quantum devices in supervised learning tasks. Among the various paradigms explored, quantum kernel methods have emerged as a particularly appealing approach due to their conceptual simplicity and natural compatibility with noisy intermediate-scale quantum (NISQ) hardware. By embedding classical data into quantum states and estimating inner products in an implicit feature space, quantum kernels provide a principled bridge between classical learning theory and quantum computation [1, 2].

Despite this promise, it is now well understood that the practical performance of quantum kernel methods is strongly influenced by the choice of data encoding. Recent studies have shown that kernel behavior is often dominated not by the quantum model itself, but by how classical data are mapped into the quantum feature space [3]. Inappropriate encodings can lead to trivial kernels, excessive concentration, or poor generalization, thereby obscuring any potential quantum advantage [4]. As a result, the design of informative and noise-resilient encodings has become a central challenge for quantum kernel methods in realistic regimes.

At the same time, there is growing recognition that quantum advantage should not be treated as a universal or binary objective. Rather than focusing exclusively on outperforming classical baselines, recent work emphasizes identifying regimes in which quantum models are practically viable, interpretable, and robust under noise and finite sampling [1, 5]. From this perspective, understanding how quantum pipelines degrade under controlled perturbations is at least as important as reporting peak performance.

A recurring insight in this line of research is the importance of *structure-aware* quantum kernels. Encodings that respect symmetries, invariances, or internal organization of the data have been shown to mitigate kernel concentration and improve robustness [6]. These observations suggest that incorporating inductive bias at the encoding stage is a promising strategy for enhancing the practical utility of quantum kernels, particularly in the NISQ regime.

In classical machine learning, one of the most successful ways to introduce such inductive bias is through preprocessing. Techniques such as principal component analysis (PCA) or frequency-domain representations based on the discrete Fourier transform (DFT) are routinely used to denoise data, reduce dimensionality, and expose global structure. In particular, spectral representations have proven especially effective for structured data such as

time series, signals, and images, where meaningful patterns often manifest more clearly in the frequency domain. While these ideas are well established classically, their systematic integration into quantum kernel pipelines remains comparatively underexplored.

Motivated by these observations, this work focuses on the role of spectral structure in quantum kernel methods. We introduce *Spectral Phase Encoding* (SPE), a frequency-aware encoding that combines a discrete Fourier transform with diagonal quantum gates to encode spectral coefficients as phases. This choice leverages the natural expressivity of diagonal unitaries while preserving the global structure revealed by spectral preprocessing.

Rather than aiming to maximize accuracy at a fixed noise level, we adopt a noise-aware evaluation strategy that explicitly characterizes how performance degrades as noise increases. Through a systematic experimental study on synthetic benchmarks, real-world datasets, and real quantum hardware, we analyze when spectral phase encoding is beneficial, when its advantages vanish, and how it behaves under realistic device noise. This approach allows us to delineate the scope of applicability and limitations of SPE in a principled and empirically grounded manner.

Related Work Quantum kernel methods were initially formalized as learning algorithms operating in implicit quantum feature spaces, enabling non-linear classification through inner products estimated on quantum devices [1, 2]. This formulation established a direct connection between classical kernel theory and quantum computation, and motivated a broad line of research on the design, evaluation, and deployment of quantum kernels under realistic conditions.

Subsequent work has investigated the feasibility of training and deploying quantum kernels on near-term hardware. In particular, Hubregtsen et al. demonstrated that quantum embedding kernels can be trained on noisy devices, while highlighting the strong sensitivity of kernel performance to hardware noise, finite sampling, and circuit depth [7]. Related studies have emphasized that practical performance is often limited not by the expressivity of the quantum model itself, but by the interaction between the chosen encoding, noise processes, and measurement statistics.

A parallel line of work has focused on improving the efficiency and scalability of quantum kernel methods. Sahin et al. proposed sub-sampling strategies to reduce the computational cost of kernel alignment and training, enabling larger-scale experiments within realistic resource budgets [8]. Variational and hybrid approaches, such as approximate or trainable QSVM

formulations, have also been explored as a means of balancing expressivity and resource requirements in the NISQ regime [9].

Beyond discrete-variable encodings, continuous-variable quantum kernels have been investigated as an alternative approach to representing classical data, offering greater flexibility at the cost of increased experimental complexity [10]. Across both discrete- and continuous-variable settings, a recurring limitation is the phenomenon of kernel concentration, whereby quantum kernels become nearly constant and lose discriminative power as system size, data dimension, or noise levels increase [4]. This observation has motivated the development of structure-aware and symmetry-respecting kernels, which incorporate inductive bias at the encoding stage to mitigate concentration effects and improve robustness [6].

The importance of data encoding has been further underscored by theoretical studies analyzing the expressive power and inductive bias of quantum feature maps. It has been shown that the choice of encoding can fundamentally determine whether a quantum kernel exhibits meaningful variability or collapses to a trivial regime, independently of the downstream learning algorithm [3, 1]. These results highlight encoding design as a central bottleneck for practical quantum kernel methods.

In classical machine learning, the introduction of inductive bias is often achieved through preprocessing. Techniques such as principal component analysis (PCA) and frequency-domain representations based on the discrete Fourier transform (DFT) are routinely used to reduce dimensionality, suppress noise, and expose global structure in data. Spectral representations, in particular, play a central role in time series analysis, signal processing, and image modeling, where relevant information often manifests more clearly in the frequency domain. Recent advances in classical learning have further reinforced the effectiveness of frequency-aware representations for structured data.

Despite their widespread use in classical pipelines, such preprocessing strategies have received comparatively limited attention in the context of quantum kernel methods. Most existing quantum encodings operate directly on raw or minimally processed features, without explicitly exploiting spectral structure or other domain-specific regularities. As a result, the potential benefits of combining classical structure-extracting transformations with quantum feature maps remain insufficiently characterized.

The present work builds on these insights by investigating spectral structure as a concrete and widely applicable source of inductive bias for quantum kernel encodings. Rather than proposing a new kernel learning paradigm, we focus on systematically characterizing how frequency-aware phase encod-

ings behave under increasing noise and realistic hardware constraints, and on identifying the regimes in which such structure-aware encodings remain informative.

2 Methods

2.1 Spectral Phase Encoding

We introduce *Spectral Phase Encoding* (SPE), a structured quantum kernel construction that combines a discrete Fourier transform (DFT) front-end with a diagonal-gate-based phase embedding. SPE is designed to exploit a structural synergy between spectral representations and phase-only quantum encodings. Throughout the experimental section, this construction is denoted as QK-DFT to emphasize the separation between classical front-end and quantum backend within the unified regression framework used for robustness analysis.

The design of SPE is motivated by two complementary observations. First, many real-world datasets exhibit meaningful structure in the frequency domain, which can be revealed through classical spectral transformations. Second, diagonal quantum gates provide a natural and hardware-efficient mechanism for encoding relative phase information, which plays a central role in quantum interference-based representations.

Classical machine learning has long exploited frequency-domain representations as a form of preprocessing or feature extraction, particularly in signal processing, time-series analysis, and image-based tasks. DFT and related spectral representations are commonly used to concentrate structured information into a reduced number of components, highlighting periodicities, global correlations, and scale-dependent patterns [11, 12]. Recent work in deep learning for time series has further emphasized the role of Fourier front-ends as a means of exposing inductive biases related to shift-invariance and long-range dependencies [13].

Given an input vector $x \in \mathbb{R}^d$, SPE begins by applying a DFT, yielding a set of complex spectral coefficients that encode global correlations and oscillatory patterns present in the data. Rather than treating the DFT as part of a trainable model, as in frequency-aware neural architectures, here it is used explicitly as a fixed preprocessing step that defines the representation supplied to the quantum embedding. This design mirrors classical pipelines in which spectral features are computed prior to classification or kernel evaluation [11].

Let $F(x) \in \mathbb{C}^d$ denote the discrete Fourier transform of x . We retain

the first m spectral components and construct a phase vector $\phi \in [-\pi, \pi)^m$, obtained from the arguments of the complex coefficients, optionally modulated by a bounded function of their magnitudes. These phases define the diagonal unitary in Eq. (1), which is applied to a uniform superposition state prepared by Hadamard gates.

$$D(\phi) = \text{diag}\left(e^{i\phi_0}, e^{i\phi_1}, \dots, e^{i\phi_{m-1}}\right), \quad (1)$$

which is applied to a uniform superposition state prepared by Hadamard gates. Diagonal unitaries admit particularly efficient decompositions, often avoiding ancilla overhead and enabling low-depth implementations [14]. When m is not a power of two, the phase vector is deterministically padded, allowing the encoding to be implemented using $n = \lceil \log_2 m \rceil$ qubits.

The resulting quantum state takes the form:

$$|\psi(x)\rangle = \frac{1}{\sqrt{2^n}} \sum_{j=0}^{2^n-1} e^{i\phi_j(x)} |j\rangle, \quad (2)$$

where $\phi_j(x)$ denotes either a retained or padded phase component. This construction highlights a key advantage of diagonal-gate-based embeddings: 2^n effective features are represented using only n qubits, without requiring state preparation procedures whose depth scales with the data dimension. In contrast to amplitude encoding, which requires normalization and multi-qubit controlled operations, SPE relies exclusively on single-qubit Hadamards and a single diagonal unitary, resulting in shallow circuits that are well aligned with current NISQ hardware constraints [2]. Moreover, in superconducting platforms, Z -axis phase rotations are commonly implemented as “virtual- Z ” updates with effectively zero duration and high fidelity, making phase/diagonal constructions especially hardware-friendly [15, 16, 17].

From a mathematical perspective, the combination of a Fourier front-end with phase-only encoding is particularly natural. The Fourier transform diagonalizes convolutional and shift-invariant operators, concentrating structured information into a reduced number of spectral modes. Encoding this information as relative phases preserves interference patterns while remaining invariant under global amplitude rescaling. Physically, diagonal gates implement relative phase accumulation with reduced reliance on entangling operations, which mitigates circuit depth and exposure to multi-qubit noise on NISQ devices [15, 16].

In this work, SPE refers specifically to the combination of a DFT front-end with a diagonal-gate-based phase embedding. To isolate the contribution of the spectral structure, we also evaluate alternative front-ends—principal

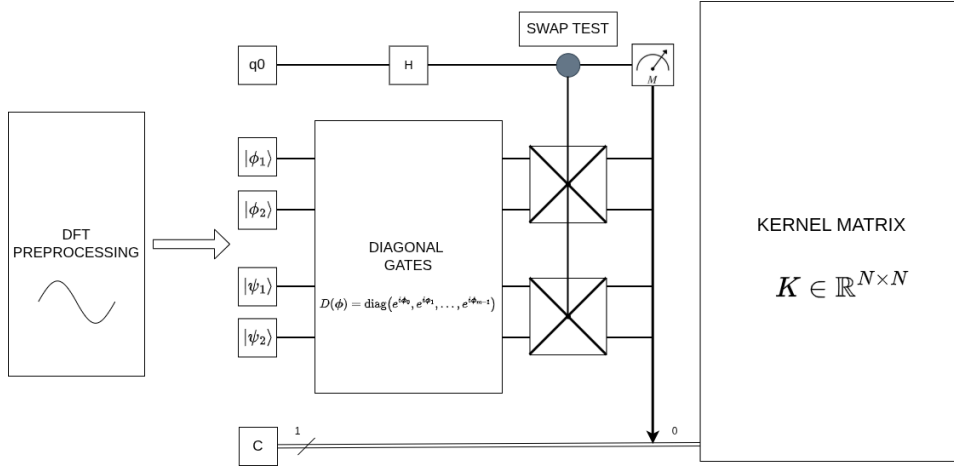


Figure 1: Conceptual pipeline of Spectral Phase Encoding. Classical data are transformed to the frequency domain, mapped to a vector of relative phases, and embedded into a quantum state using a diagonal gate acting on a uniform superposition. Kernel values are obtained via overlap estimation.

component analysis (PCA) and random projections (RP)—under the same diagonal quantum embedding, leading to the constructions QK-PCA and QK-RP in the experimental section. This controlled comparison enables us to disentangle the effect of spectral preprocessing from that of the quantum embedding itself.

Finally, kernel values are obtained by estimating overlaps between SPE-encoded quantum states using a SWAP test. This choice ensures direct compatibility with quantum kernel methods while maintaining a clear separation between classical preprocessing, quantum state preparation, and kernel evaluation. A schematic overview of the full SPE pipeline is shown in Fig. 1.

Remark 1 (Phase-only encodings and complex-valued features). *A practical motivation for diagonal-gate-based phase encoding is its natural compatibility with complex-valued features. Spectral representations produced by the discrete Fourier transform are inherently complex, with relevant information encoded in both magnitude and phase. Most standard quantum feature maps, including amplitude and angle encodings, are defined for real-valued inputs and therefore require ad hoc transformations or the explicit discarding of complex phase information [1, 2]. By contrast, diagonal quantum gates natively implement relative phase shifts, providing a direct and hardware-*

efficient mechanism to encode complex phases. This makes phase-only encodings particularly well suited for spectral representations and allows the Fourier front-end in SPE to be integrated without additional approximations, while preserving a low-depth, NISQ-compatible circuit structure.

2.2 Kernel evaluation and learning protocol

All feature constructions considered in this work are evaluated within the same kernel-based learning framework. Given a dataset $\{(x_i, y_i)\}_{i=1}^N$, classical preprocessing is first applied to obtain a transformed representation for each input, which is subsequently mapped to a quantum state using the chosen feature construction. Kernel values are then obtained by estimating pairwise state overlaps.

For a given training set, we construct a kernel matrix $K \in \mathbb{R}^{N \times N}$, where each entry K_{ij} corresponds to the estimated overlap between the quantum states associated with x_i and x_j . To mitigate trivial correlations and improve numerical stability, kernel matrices are centered prior to downstream evaluation. Centered kernels are used consistently for all diagnostic metrics and learning tasks.

Learning performance is assessed using a support vector machine (SVM) with a precomputed kernel. Train–test splits are generated using stratified sampling to preserve class balance, and all reported metrics are averaged over multiple random seeds. This protocol ensures that observed performance differences reflect systematic effects of the feature construction rather than artifacts of a particular data split.

In addition to classification accuracy and macro-averaged F1 score, we report kernel-level diagnostics that provide insight into representation quality. Specifically, we compute kernel alignment with the ideal label kernel, as well as the difference between within-class and between-class similarities. These quantities characterize how well the induced kernel geometry reflects class structure independently of the classifier.

To analyze robustness under noise, kernel construction and evaluation are repeated across a range of noise levels. Noise is injected at the data level prior to preprocessing, ensuring that all methods are exposed to identical perturbations. This design isolates the effect of the feature construction on robustness and allows degradation trends to be compared in a controlled and reproducible manner.

Unless stated otherwise, the same evaluation protocol is used for all classical front-ends and quantum feature maps, enabling a fair and systematic comparison.

2.3 Experimental setup

Our empirical evaluation spans 20 widely used image-like classification benchmarks covering heterogeneous visual regimes (e.g., digits, natural images, faces, and medical imagery). These datasets are commonly employed in both classical and quantum machine learning studies, enabling reproducible and externally comparable robustness assessments 5. To make results comparable across datasets with different native resolutions and formats, all inputs are converted to grayscale when applicable, rescaled to a common 32×32 resolution, and normalized to $[0, 1]$ prior to feature construction. For each noise level we subsample $N = 150$ examples using class-balanced sampling to prevent spurious shifts in effective class priors. Dataset metadata (classes and characteristics) are reported in Appendix A (Table 2).

Robustness is assessed under controlled additive Gaussian corruption applied to normalized inputs,

$$x \mapsto \text{clip}_{[0,1]}(x + \eta), \quad \eta \sim \mathcal{N}(0, \sigma^2), \quad (3)$$

with $\sigma \in \{0.00, 0.025, 0.05, 0.075, 0.10, 0.125, 0.15, 0.20\}$. The upper bound $\sigma = 0.20$ corresponds to perturbations with variance 0.04 in the $[0, 1]$ domain, representing a high-noise regime where structure is significantly degraded but not fully destroyed, thereby enabling slope-based robustness comparisons before universal chance-level collapse.

To isolate the role of the feature construction, we evaluate a family of quantum-kernel and classical-kernel pipelines that share the same downstream classifier (SVM with a precomputed kernel) and differ only in the classical front-end that generates the m -dimensional representation feeding the quantum embedding. We consider three standard and widely adopted front-end constructions in machine learning: a DFT-based spectral selection, principal component analysis (PCA), and random projections (RP). These represent, respectively, frequency-domain feature extraction, variance-maximizing linear compression, and structure-agnostic dimensionality reduction. To ensure a controlled comparison, we tie the retained feature dimension to the quantum state dimension, $m = 2^n$, so that all variants operate at identical effective dimensionality for fixed circuit size. DFT features are selected using a low-frequency radial criterion in 2D Fourier space, while PCA and RP are constructed to match the same m .

Kernel entries are estimated via quantum overlap estimation using a fixed number of circuit repetitions (shots), i.e., repeated projective measurements used to estimate expectation values under finite sampling. This fixed shot budget ensures comparable statistical precision across all vari-

ants, producing K_{tr} and $K_{\text{te, tr}}$; an SVM is trained using the precomputed kernel. All normalization statistics and any diagnostic kernel quantities are computed strictly on training data to prevent leakage [18]. We use stratified train–test splits with a 30% test fraction, repeated over five random seeds; performance metrics are averaged across seeds.

A central difficulty in cross-method robustness comparisons is that each dataset admits multiple valid configurations (e.g., different n and associated m , and possibly different budgets). To provide a fair comparison while allowing each method family to operate in a realistic tuned regime, we adopt a clean-data hyperparameter selection protocol. Specifically, for each dataset d and each method group g , we select the configuration that maximizes mean accuracy at a reference noise level σ_0 (here $\sigma_0 = 0$), and then freeze that choice for all $\sigma \in \mathcal{S}$. This mirrors standard practice in which hyperparameters are tuned on clean (or lightly corrupted) data and robustness is assessed out-of-distribution, while explicitly avoiding noise-dependent retuning.

In particular, the group denoted QK_DFT corresponds to the SPE construction introduced in Sec. 2.1. Under this protocol we compare five groups within a single unified statistical framework: QK_DFT (i.e., SPE), QK_PCA, and QK_RP—three quantum kernels sharing the same diagonal embedding but differing in their classical front-end—and two classical baselines, SVM_Linear and SVM_RBF, evaluated under the same preprocessing choice used in the classical branch. Robustness is quantified using a dataset fixed-effects regression model with group-specific degradation slopes. Taking QK_DFT as the reference group, we fit

$$\text{Acc}_i = \alpha_{d(i)} + \beta_{\text{QK-DFT}} \sigma_i + \sum_{g \neq \text{QK-DFT}} \delta_g \sigma_i \mathbf{1}_{g(i)} + \varepsilon_i, \quad (4)$$

so that each group has slope $\beta_g = \beta_{\text{QK-DFT}} + \delta_g$. Inference is performed with a wild cluster bootstrap using Rademacher weights at the dataset level ($B = 4000$ replications), which preserves within-dataset dependence and yields robust confidence intervals for slope differences. For visualization, we report accuracy–vs–noise curves after σ_0 selection, together with bootstrap median curves and 95% bands to reflect between-dataset variability.

Finally, to validate practical executability, we conduct a hardware micro-benchmark on IBM Quantum backends using a SWAP-test overlap estimation task (Sec. 3.3). The objective is not end-to-end classification on hardware, but to assess overlap-estimation stability under realistic compilation and gate noise.

3 Results

The primary objective of this study is to characterize how different feature constructions degrade as input noise increases, thereby providing a robustness-centered evaluation rather than a peak-accuracy comparison. In realistic machine learning pipelines—particularly in hybrid quantum-classical settings—data corruption is unavoidable, and performance stability under perturbations is often more relevant than peak clean accuracy. Consequently, evaluating methods at a single noise level can be misleading: a model that performs strongly at $\sigma = 0$ but deteriorates rapidly may be less desirable than a model with slightly lower clean accuracy but substantially greater robustness.

In this context, comparing methods solely at a fixed noise level can be misleading. A method that achieves high accuracy at low noise but deteriorates rapidly may be less desirable than a method that exhibits slightly lower peak performance but degrades more gracefully. Accordingly, we adopt a noise-aware evaluation strategy in which the noise level σ is treated as a controlled experimental variable, and performance is analyzed as a function of increasing noise. Note that the underlying benchmark datasets already contain inherent acquisition and preprocessing noise; the added Gaussian perturbation therefore represents controlled incremental corruption rather than a transition from perfectly clean data. This evaluation strategy is consistent with established corruption-robustness benchmarks in computer vision. As surveyed in [19], corruption benchmarks such as CIFAR-C and ImageNet-C, originally introduced by Hendrycks and Dietterich [20], systematically apply controlled levels of common perturbations—including Gaussian noise, blur, and digital distortions—to clean datasets in order to quantify performance degradation under distribution shift.

All results in this section are constructed under a unified experimental protocol described in Sec. 2.3. In particular, hyperparameters are selected at a clean reference noise level $\sigma_0 = 0$ separately for each dataset and method group, and then frozen for all higher noise levels. This prevents noise-dependent retuning and mirrors standard practice in which models are tuned on clean data and evaluated under distribution shift. Robustness is then quantified through a dataset fixed-effects regression model with group-specific degradation slopes, using wild cluster bootstrap inference at the dataset level.

We jointly compare five method groups within a single regression framework: QK_DFT, QK_PCA, QK_RP, SVM_Linear, and SVM_RBF. QK_DFT (spectral preprocessing followed by diagonal quantum encoding) is treated

as the reference group. This unified modeling approach ensures that all slope estimates and confidence intervals arise from the same statistical experiment, avoiding inconsistencies that can arise from method-specific aggregation rules.

Throughout this section, we present complementary views of robustness. First, we report global degradation slopes obtained from the fixed-effects regression, which quantify accuracy loss per unit increase in σ . These slopes provide a compact and statistically grounded summary of robustness differences across methods. Second, we present accuracy-versus-noise curves with bootstrap confidence bands, offering a more granular visualization of degradation trajectories. Together, these analyses provide both quantitative and descriptive evidence regarding relative robustness.

Importantly, our analysis focuses on regimes in which performance degradation remains informative, rather than on asymptotic collapse scenarios. The emphasis is therefore on comparative stability across increasing corruption levels, rather than on characterizing trivial high-noise behavior. In this way, the results directly address the central question of this work: whether spectral preprocessing combined with diagonal quantum encoding yields a more favorable degradation profile than alternative classical or quantum feature constructions under controlled noise.

3.1 Performance Evolution under Noise

We first analyze how classification accuracy evolves as a function of increasing additive Gaussian noise under the clean-data hyperparameter selection protocol described in Sec. 2.3. The visual evolution of the corrupted inputs corresponding to increasing σ is illustrated in Appendix A.2 (Fig. 6). As the noise standard deviation σ increases, spatial structure progressively degrades, eventually approaching visually uninformative patterns. The quantitative impact of this degradation on classification performance is shown in Fig. 2.

Figure 2 reports accuracy-vs-noise curves for four representative datasets spanning natural images, handwritten digits, face recognition, and medical imaging. For each dataset and each method group, the configuration achieving the highest mean accuracy at $\sigma_0 = 0$ is selected and then *frozen* for all subsequent noise levels. This mirrors standard practice in which hyperparameters are tuned on clean data and robustness is evaluated out-of-distribution without noise-dependent retuning.

Across datasets, a consistent qualitative pattern emerges. Among the quantum variants, QK_DFT exhibits a systematically milder degradation

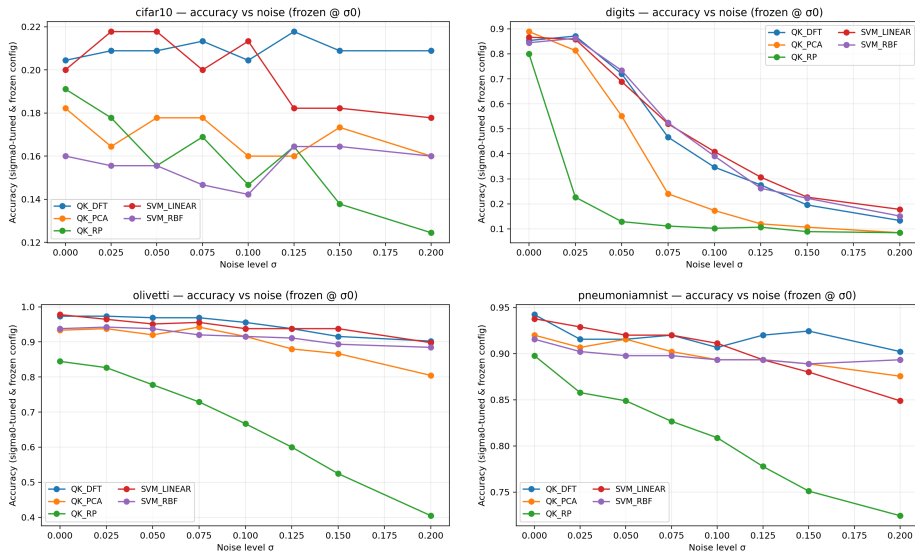


Figure 2: Accuracy vs noise level σ for four representative datasets under σ_0 -frozen configuration selection.

compared to QK_PCA and especially QK_RP, whose slopes are visibly steeper as σ increases. The classical baselines (SVM_Linear and SVM_RBF) display intermediate behavior, with degradation patterns that vary across datasets but do not systematically outperform QK_DFT in the moderate-noise regime.

To assess this behavior at scale, we aggregate winner counts across all 20 datasets at each noise level using the frozen-configuration protocol. Figure 3 reports the number of datasets for which each method achieves the highest accuracy at each σ .

QK_DFT achieves the largest number of wins across most noise levels, particularly in the intermediate corruption regime ($0.05 \leq \sigma \leq 0.15$), where structural information remains partially preserved but fine details are increasingly distorted. In this range, QK_DFT attains between 7 and 8 wins out of 20 datasets, consistently matching or exceeding the performance of the classical baselines. In contrast, QK_PCA and especially QK_RP exhibit markedly fewer wins across the spectrum, reflecting their steeper degradation patterns observed in the per-dataset curves. While SVM_Linear and SVM_RBF occasionally achieve competitive or even leading performance at specific noise levels (notably at $\sigma = 0$ and $\sigma = 0.05$), no consistent dominance over QK_DFT emerges as noise increases.

Taken together, these aggregated winner counts indicate that the Fourier-

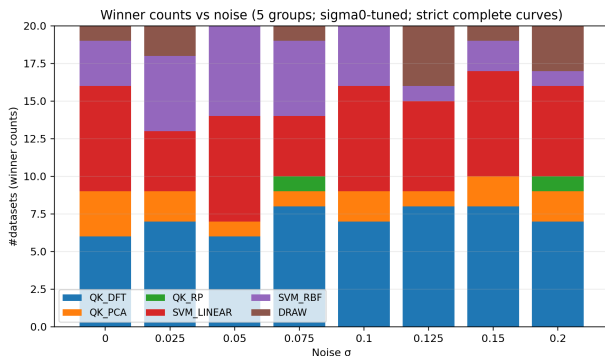


Figure 3: Number of datasets (out of 20) for which each method achieves the highest accuracy at each noise level σ , after clean-data configuration selection and freezing.

based quantum construction (QK_DFT) maintains a comparatively stable competitive position under corruption. Rather than relying on isolated peak accuracies, the advantage manifests as sustained top performance across a broad noise range, suggesting that the combination of spectral preprocessing and diagonal phase embedding yields a robustness profile that is not systematically surpassed by alternative quantum front-ends or classical kernel baselines under the same clean-data tuning protocol.

3.2 Noise robustness analysis

We now quantify robustness using the regression framework introduced in Sec. 2.3, applied to the σ_0 -tuned configurations of all five method groups simultaneously. Robustness is measured by the degradation slope β_g , defined as the change in accuracy per unit increase of noise level σ .

Figure 4 summarizes the results. Panel (a) reports the estimated slopes with 95% wild cluster bootstrap confidence intervals (clustered at the dataset level, $B = 4000$), and Panel (b) shows the corresponding aggregated accuracy curves with bootstrap bands. Numerical estimates are provided in Table 1.

Table 1: Noise robustness slopes estimated via dataset fixed-effects regression with wild cluster bootstrap. Slopes correspond to accuracy change per unit increase in noise σ . QK-DFT is the reference category.

Parameter	Estimate	CI _{95%} Low	CI _{95%} High	Pr($\beta < 0$)
$\beta_{\text{QK-DFT}}$	-0.214	-0.645	0.222	0.801
$\beta_{\text{QK-PCA}}$	-0.568	-1.063	-0.075	0.995
$\Delta(\text{QK-PCA} - \text{QK-DFT})$	-0.354	-0.524	-0.188	1.000
$\beta_{\text{QK-RP}}$	-1.367	-1.962	-0.760	1.000
$\Delta(\text{QK-RP} - \text{QK-DFT})$	-1.153	-1.592	-0.707	1.000
$\beta_{\text{SVM-Linear}}$	-0.253	-0.630	0.118	0.867
$\Delta(\text{SVM-Linear} - \text{QK-DFT})$	-0.040	-0.179	0.093	0.714
$\beta_{\text{SVM-RBF}}$	-0.362	-0.769	0.041	0.948
$\Delta(\text{SVM-RBF} - \text{QK-DFT})$	-0.149	-0.289	-0.011	0.986

$$\begin{aligned}
 \beta_{\text{QK-DFT}} &= -0.214, \\
 \beta_{\text{QK-PCA}} &= -0.568, \\
 \beta_{\text{QK-RP}} &= -1.367, \\
 \beta_{\text{SVM-Linear}} &= -0.253, \\
 \beta_{\text{SVM-RBF}} &= -0.362.
 \end{aligned}$$

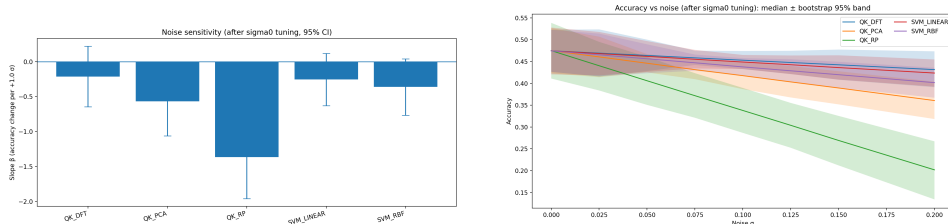
Within the quantum family, DFT-based encoding exhibits the smallest degradation rate, while PCA and especially random projections deteriorate substantially faster. The differences relative to QK-DFT are:

$$\begin{aligned}
 \Delta(\text{QK-PCA} - \text{QK-DFT}) &= -0.354, \\
 \Delta(\text{QK-RP} - \text{QK-DFT}) &= -1.153,
 \end{aligned}$$

with bootstrap confidence intervals strictly below zero, indicating a statistically robust advantage of spectral preprocessing within quantum models.

When compared to classical baselines, QK-DFT displays a degradation rate comparable to linear SVM and more favorable than RBF SVM. In particular:

$$\begin{aligned}
 \Delta(\text{SVM-Linear} - \text{QK-DFT}) &= -0.040, \\
 \Delta(\text{SVM-RBF} - \text{QK-DFT}) &= -0.149.
 \end{aligned}$$



(a) Noise sensitivity by method. Bars show the estimated degradation slopes β (accuracy change per unit increase in noise σ), with 95% wild cluster bootstrap confidence intervals (clustered by dataset, $B = 4000$).

(b) Global accuracy vs noise level σ aggregated across complete dataset–configuration curves. Lines show the bootstrap median and shaded regions indicate the 95% wild cluster bootstrap bands (clustered by dataset, $B = 4000$).

Figure 4: Global robustness analysis. (a) Degradation slopes with bootstrap confidence intervals. (b) Aggregated accuracy curves with 95% bootstrap bands.

The linear SVM difference is not statistically significant, whereas the RBF SVM exhibits significantly stronger degradation under noise.

Taken together, these results show that robustness is strongly governed by preprocessing alignment: spectral (DFT) representations yield consistently smaller noise sensitivity both in quantum and classical settings. However, the diagonal quantum feature map preserves this stability and avoids the stronger degradation observed in nonlinear classical kernels under the same spectral features.

3.3 Hardware validation: overlap estimation under realistic noise

To complement the simulation-based robustness analysis, we assess the practical executability of SPE—denoted QK-DFT in the unified regression framework—on current superconducting quantum hardware. Rather than performing end-to-end classification on hardware, which would confound kernel behavior with training variance and limited shot budgets, we isolate the fundamental primitive underlying the quantum kernel: state overlap estimation. Given two real-valued inputs (x, y) with prescribed cosine similarity ρ , we prepare the corresponding quantum states $|\psi(x)\rangle$ and $|\psi(y)\rangle$ using the SPE construction (QK-DFT) or a low-depth angle-encoding baseline. The overlap is estimated via a SWAP test, producing a hardware probability

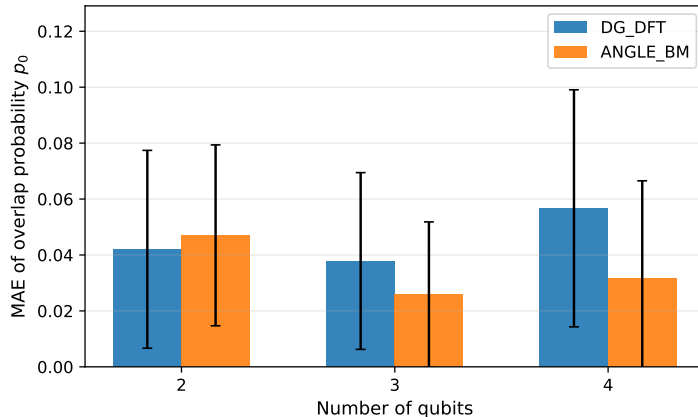


Figure 5: Hardware overlap-estimation error across qubit sizes. Mean absolute error (MAE) of $|\Delta p_0| = |p_0^{\text{hw}} - p_0^{\text{exp}}|$ for SPE (DFT + DiagonalGate) and a low-depth angle-encoding baseline, averaged over two IBM Quantum backends (`ibm_fez`, `ibm_marrakesh`), similarity values, and repeated runs. Error bars indicate variability across measurement instances.

p_0^{hw} , which we compare against its expected reference value p_0^{exp} obtained from analytic calculation (SPE) or noiseless statevector simulation (angle baseline). Hardware fidelity is summarized through the absolute deviation

$$|\Delta p_0| = |p_0^{\text{hw}} - p_0^{\text{exp}}|,$$

which directly measures how accurately the device reproduces the theoretical kernel overlap.

Experiments were executed on two distinct IBM Quantum backends, `ibm_fez` and `ibm_marrakesh`, using identical circuit constructions, transpilation strategies, and shot budgets. Results are averaged across backends, multiple similarity settings, and repeated runs in order to mitigate backend-specific calibration fluctuations and transient noise effects.

Figure 5 reports the mean absolute error as a function of qubit count. Across all tested regimes ($n = 2, 3, 4$), deviations remain moderate and do not exhibit catastrophic growth with increasing system size. Although the relative ordering between SPE and the angle baseline varies with qubit count, both constructions produce stable and non-degenerate overlap estimates. Importantly, the diagonal phase embedding does not display instability or collapse as circuit depth increases, despite relying on structured phase accumulation across computational basis states.

These results provide empirical evidence that the structural properties exploited by SPE—namely diagonal phase encoding and low entangling depth—translate into hardware executability on present-day superconducting devices. Combined with the large-scale simulation analysis, this hardware validation supports the practical viability of SPE as a kernel-construction mechanism compatible with current NISQ architectures.

4 Discussion

This work reframes the evaluation of quantum kernel constructions from peak clean-data performance toward controlled degradation under distributional corruption. Rather than asking whether a given encoding achieves the highest accuracy at $\sigma = 0$, we quantify how performance decays as additive noise increases, and compare degradation rates across quantum and classical pipelines under matched tuning conditions. This perspective is consistent with recent arguments that quantum advantage should not be framed as a binary outcome, but assessed through stability, structural alignment, and feasibility under realistic NISQ constraints [1, 5].

Methodologically, the study integrates three elements into a single robustness framework: (i) clean-data hyperparameter selection with frozen configurations, (ii) dataset fixed-effects regression with group-specific noise slopes, and (iii) wild cluster bootstrap inference at the dataset level. This design prevents optimistic noise-dependent retuning and avoids overconfident inference due to repeated measurements within datasets. In contrast to descriptive degradation plots alone, the regression model yields interpretable slope coefficients β_g representing accuracy loss per unit noise increase, enabling direct cross-family comparison.

Across the five model families considered (QK-DFT, QK-PCA, QK-RP, SVM-Linear, SVM-RBF), a consistent structure emerges. Within the quantum family, QK-DFT exhibits the smallest degradation magnitude, followed by QK-PCA and then QK-RP. The slope differences between QK-PCA and QK-DFT, and especially between QK-RP and QK-DFT, are supported by bootstrap intervals excluding zero, indicating a statistically robust advantage of Fourier-based preprocessing within the diagonal quantum embedding. By contrast, QK-PCA and QK-RP degrade substantially faster as corruption increases.

The particularly steep degradation observed for random projections is consistent with classical dimensionality-reduction theory. While random projections preserve pairwise distances in expectation under Johnson- Lin-

denstrauss guarantees [21, 22], they do not exploit data-dependent or task-aligned structure. Under additive noise, this structure-agnostic property provides no preferential preservation of discriminative directions, leading to accelerated collapse relative to variance-based (PCA) or frequency-aware (DFT) representations. PCA, by construction, concentrates maximal variance directions [23, 24], which partially explains its intermediate robustness profile.

The favorable behavior of QK-DFT can be interpreted through the interaction between spectral preprocessing and diagonal unitary feature maps. Fourier-domain representations have repeatedly been shown to act as an inductive bias in classical learning, improving robustness and expressivity in noisy image and signal settings [25, 26, 27, 28]. Injecting this spectral structure into a phase-only diagonal quantum embedding preserves interference-based relational information without increasing circuit depth. Diagonal encodings are known to be hardware-compatible and shallow relative to more entanglement-heavy constructions [29, 2], and recent analyses emphasize the importance of structure-aware and symmetry-respecting feature maps for avoiding kernel concentration and expressivity pathologies [6, 30]. Our results suggest that the combination of Fourier structure and diagonal phase encoding provides a favorable compromise between expressivity and stability under corruption.

Importantly, the comparison with classical SVM baselines clarifies that robustness gains are not purely a consequence of preprocessing. When evaluated under identical clean-data tuning, QK-DFT exhibits a degradation rate comparable to linear SVM and more stable than RBF SVM under the same spectral preprocessing. This indicates that robustness is jointly governed by representation alignment and the geometry induced by the kernel map, rather than by the classical front-end alone.

The hardware validation further supports the practical viability of this construction. While QK-DFT does not uniformly outperform a low-depth angle-encoding baseline in absolute overlap-estimation error, it remains numerically stable across qubit counts and backends. Given the well-known sensitivity of hardware experiments to calibration, transpilation, and backend-specific noise profiles [7, 31], the key observation is that the diagonal phase construction does not exhibit instability or collapse under realistic device noise. This operational stability is consistent with its shallow, diagonal structure and supports its suitability for near-term quantum kernel pipelines.

Overall, the findings position Spectral Phase Encoding as a structurally aligned quantum feature construction whose advantage lies not in universal peak accuracy, but in slower degradation under corruption and in statisti-

cally supported slope improvements within the quantum family. The results also highlight that robustness is fundamentally domain-conditional: spectral alignment benefits datasets exhibiting exploitable frequency structure, while offering limited gains when such structure is weak. This nuanced picture aligns with the broader shift in quantum machine learning toward domain-aware, noise-conscious algorithm design, where progress is likely to depend less on universal advantage claims and more on identifying structurally compatible problem classes.

5 Conclusion

We introduced Spectral Phase Encoding (SPE), a hybrid quantum feature construction that combines a discrete Fourier transform (DFT) front-end with a phase-only diagonal quantum embedding. Within the unified experimental framework, this construction is instantiated as QK-DFT and evaluated alongside alternative quantum front-ends (QK-PCA, QK-RP) and classical SVM baselines under a common clean-data tuning protocol.

Rather than focusing on peak accuracy at zero noise, the central objective of this study was to characterize controlled degradation under additive corruption. By combining clean-data hyperparameter selection, dataset fixed-effects regression, and wild cluster bootstrap inference, we quantified robustness through interpretable degradation slopes across 20 heterogeneous datasets.

The results consistently show that within the quantum family, QK-DFT exhibits the smallest magnitude degradation under increasing noise, followed by QK-PCA and QK-RP. The slope differences relative to QK-DFT are statistically supported by bootstrap intervals excluding zero, indicating a robust advantage of spectral preprocessing within a diagonal quantum embedding. Importantly, when compared to classical SVM baselines under identical tuning conditions, QK-DFT displays a degradation rate comparable to linear SVM and more stable than RBF SVM, suggesting that robustness arises from the interaction between representation alignment and kernel geometry rather than from preprocessing alone.

These findings are consistent with theoretical analyses indicating that quantum kernels can suffer from expressivity collapse and concentration phenomena under noise and measurement constraints [4]. By injecting structured spectral information into a shallow diagonal embedding, SPE provides a construction that balances expressivity and stability without increasing circuit depth. From a hardware perspective, diagonal phase constructions

remain particularly attractive on superconducting platforms, where virtual- Z implementations and shallow diagonal synthesis reduce overhead and systematic error [15, 16, 17, 14].

The hardware experiments further demonstrate that SPE (QK-DFT) remains operational across multiple backends and qubit counts, producing stable overlap estimates without evidence of catastrophic degradation. While not implying hardware-level dominance, this stability reinforces the practical compatibility of diagonal phase embeddings with present-day NISQ devices.

From a computational perspective, the classical front-ends considered here differ modestly in preprocessing cost. DFT-based spectral selection can be implemented in $O(d \log d)$ time via FFT routines, while PCA requires an initial covariance estimation and eigendecomposition, and random projections incur $O(dm)$ projection cost without training overhead. In our experimental regime, these classical costs remain negligible compared to the dominant expense of quantum kernel estimation under finite measurement shots. Consequently, the observed robustness differences cannot be attributed to disproportionate classical preprocessing complexity [32, 33, 34].

Overall, the advantage of SPE does not lie in universally higher clean-data accuracy, but in statistically supported slower degradation under corruption and in the existence of robust configurations when the data exhibit exploitable spectral structure. This supports the broader view that successful quantum kernel constructions require domain-compatible inductive bias rather than universal advantage claims [30].

Future Directions

The present results suggest several concrete extensions:

1. **Structure-aware and symmetry-respecting extensions.** Integrating SPE-style spectral priors with explicitly covariant or symmetry-aware kernel constructions may further improve stability and inductive alignment. Covariant quantum kernels provide a principled mechanism for encoding invariances and have been experimentally demonstrated in superconducting settings [6].
2. **Mitigating kernel concentration in larger regimes.** Since kernel concentration and noise-induced collapse can limit informativeness at larger scales [4], mitigation strategies tailored to fidelity-based kernels remain important. Recent proposals demonstrate practical mitigation techniques for covariant fidelity kernels at larger sizes [35].

3. **Learnable spectral selection and hybrid transforms.** SPE currently relies on fixed Fourier truncation. Extensions incorporating adaptive frequency masks, learnable phase scalings, or alternative frequency transforms (e.g., DFT/DCT/wavelets) would connect this framework to the broader frequency-based inductive bias literature in modern machine learning [12, 13, 36].
4. **Scalable kernel training and alignment.** Incorporating trainable phase scalings or diagonal layers, optimized through kernel alignment objectives, may enhance performance while controlling circuit depth. Subsampling-based alignment strategies offer a promising route to reduce training overhead [8].
5. **Hardware-aware diagonal synthesis.** As system size grows, compilation and diagonal synthesis will increasingly determine realized depth and noise sensitivity. Leveraging optimized diagonal decompositions and virtual- Z -centric compilation strategies can further reduce systematic error [15, 17, 14]. More broadly, recent analyses of Grover-based circuit constructions highlight that qubit overhead and circuit depth remain the primary bottlenecks on current NISQ hardware, even for moderately sized problem instances [37]. This reinforces the importance of shallow, structure-preserving encodings when aiming for practical scalability.
6. **Bridging to classically hard diagonal feature maps.** Integrating spectral priors with commuting or diagonal circuit families conjectured to be classically hard to simulate may strengthen separations in kernel evaluation. Complexity-theoretic evidence for commuting circuit hardness provides motivation for such exploration [38].
7. **Application-driven evaluation under realistic constraints.** While several studies report promising speedups of quantum algorithms in domains such as financial optimization, practical deployment remains limited by hardware cost, calibration instability, and circuit depth constraints [39]. Future work should therefore evaluate encoding strategies such as SPE within domain-specific pipelines under realistic hardware and resource assumptions.
8. **Error mitigation for overlap estimation.** Since kernel evaluation remains measurement-limited and noise-sensitive, incorporating mitigation techniques specifically designed for near-term fidelity estimation pipelines is an important practical direction [35].

Supplementary information The code required to reproduce all experiments, figures, and statistical analyses is publicly available at: <https://github.com/cloudlab-aia/kernel-comparison>. The repository includes data preprocessing scripts, kernel construction routines, evaluation pipelines, and instructions for reproducing the main results.

Acknowledgements Grant Serverless4HPC PID2023-152804OB-I00 funded by MICIU/AEI/10.13039/501100011033 and by ERDF/EU.

A Additional experimental details

A.1 Class selection and dataset balancing

Table 2: Overview of the 20 real-world 2D datasets used in the experiments. All datasets are converted to grayscale (when applicable), resized to 32×32 , and subsampled to a balanced subset as described in Sec. 2.3.

Dataset	Classes (C)	Domain	Source
BreastMNIST	2	Medical imaging	MedMNIST
CIFAR-10	10	Natural images	CIFAR
DermaMNIST	7	Dermatology	MedMNIST
Digits	10	Handwritten	scikit-learn
DTD	20	Texture	Oxford VGG
EMNIST (ByClass)	20	Characters	NIST
Fashion-MNIST	10	Clothing	Zalando
FER2013	7	Facial expr.	Kaggle
GTSRB	20	Traffic signs	GTSRB
KMNIST	10	Japanese char.	KMNIST
OCTMNIST	4	Retinal OCT	MedMNIST
PneumoniaMNIST	2	Chest X-ray	MedMNIST
RetinaMNIST	5	Retinal	MedMNIST
STL-10	10	Natural images	Stanford
SVHN (cropped)	10	Street digits	SVHN
USPS	10	Handwritten	LIBSVM

Real-world datasets considered in this work differ substantially in their number of available classes, class imbalance, and total sample size. To ensure a fair and reproducible comparison across datasets, we adopt a unified and deterministic class-selection rule that balances representativeness and

statistical reliability. For each dataset, we first determine the total number of available classes C_{avail} from the full label set. Unless explicitly overridden, the number of classes C used in the experiments is then selected according to the following rule:

$$C = \min\left(\left\lfloor \frac{N}{n_{\text{spc}}} \right\rfloor, C_{\text{cap}}, C_{\text{avail}}\right), \quad (5)$$

where N is the total number of samples requested for the dataset, n_{spc} is the target minimum number of samples per class, and C_{cap} is a fixed upper bound on the number of classes. In all experiments, we use $n_{\text{spc}} = 10$ and $C_{\text{cap}} = 20$.

This rule enforces three constraints simultaneously: (i) each class is represented by a sufficient number of samples to avoid degenerate decision boundaries, (ii) datasets with a very large number of classes are capped to prevent overly sparse class coverage, and (iii) the selected number of classes never exceeds the number of classes originally present in the dataset.

Once C is determined, the corresponding classes are selected deterministically using a fixed random seed. This ensures that class identities are reproducible across runs and noise levels, while avoiding any bias induced by manual class curation. Given the selected classes, a strictly class-balanced subset of N samples is then drawn using stratified sampling.

A.2 Progressive Samples Corruption

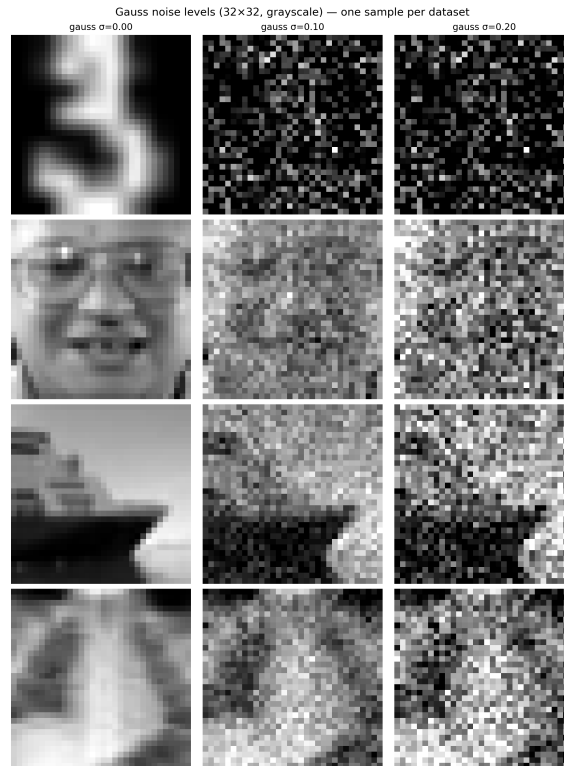


Figure 6: Representative samples under increasing Gaussian noise σ .

References

- [1] Maria Schuld and Nathan Killoran. Is Quantum Advantage the Right Goal for Quantum Machine Learning? *PRX Quantum*, 3(3):030101, July 2022.
- [2] Vojtěch Havlíček, Antonio D. Córcoles, Kristan Temme, Aram W. Harrow, Abhinav Kandala, Jerry M. Chow, and Jay M. Gambetta. Supervised learning with quantum-enhanced feature spaces. *Nature*, 567(7747):209–212, March 2019.
- [3] Minati Rath and Hema Date. Quantum data encoding: a comparative analysis of classical-to-quantum mapping techniques and their impact on machine learning accuracy. *EPJ Quantum Technology*, 11(1):72, October 2024.

- [4] Supanut Thanasilp, Samson Wang, M. Cerezo, and Zoë Holmes. Exponential concentration in quantum kernel methods. *Nature Communications*, 15(1):5200, June 2024.
- [5] Sofiene Jerbi, Lukas J. Fiderer, Hendrik Poulsen Nautrup, Jonas M. Kübler, Hans J. Briegel, and Vedran Dunjko. Quantum machine learning beyond kernel methods. *Nature Communications*, 14(1):517, January 2023.
- [6] Jennifer R. Glick, Tanvi P. Gujarati, Antonio D. Córcoles, Youngseok Kim, Abhinav Kandala, Jay M. Gambetta, and Kristan Temme. Covariant quantum kernels for data with group structure. *Nature Physics*, 20(3):479–483, March 2024.
- [7] Thomas Hubregtsen, David Wierichs, Elies Gil-Fuster, Peter-Jan H. S. Derks, Paul K. Faehrmann, and Johannes Jakob Meyer. Training quantum embedding kernels on near-term quantum computers. *Physical Review A*, 106(4):042431, October 2022.
- [8] M. Emre Sahin, Benjamin C. B. Symons, Pushpak Pati, Fayyaz Minhas, Declan Millar, Maria Gabrani, Stefano Mensa, and Jan Lukas Roberatus. Efficient Parameter Optimisation for Quantum Kernel Alignment: A Sub-sampling Approach in Variational Training. *Quantum*, 8:1502, October 2024.
- [9] Siheon Park, Daniel K. Park, and June-Koo Kevin Rhee. Variational quantum approximate support vector machine with inference transfer. *Scientific Reports*, 13(1):3288, February 2023.
- [10] Laura J. Henderson, Rishi Goel, and Sally Shrapnel. Quantum Kernel Machine Learning With Continuous Variables. *Quantum*, 8:1570, December 2024.
- [11] Ben D. Fulcher and Nick S. Jones. Highly comparative feature-based time-series classification. *IEEE Transactions on Knowledge and Data Engineering*, 2014.
- [12] Kun Yi, Qi Zhang, Wei Fan, Longbing Cao, Shoujin Wang, Hui He, Guodong Long, Liang Hu, Qingsong Wen, and Hui Xiong. A survey on deep learning based time series analysis with frequency transformation. In *Proceedings of the 31st ACM SIGKDD Conference on Knowledge Discovery and Data Mining (KDD '25)*, 2025.

- [13] Tian Zhou, Ziqing Ma, Qingsong Wen, Xue Wang, Liang Sun, and Rong Jin. Fedformer: Frequency enhanced decomposed transformer for long-term series forecasting. arXiv:2201.12740, 2022.
- [14] Jonathan Welch, Daniel Greenbaum, Sarah Mostame, and Alán Aspuru-Guzik. Efficient quantum circuits for diagonal unitaries without ancillas. *New Journal of Physics*, 16:033040, 2014.
- [15] David C. McKay, Christopher J. Wood, Sarah Sheldon, Jerry M. Chow, and Jay M. Gambetta. Efficient z gates for quantum computing. *Physical Review A*, 96(2):022330, 2017.
- [16] Morten Kjaergaard, Mollie E. Schwartz, Jochen Braumüller, Philip Krantz, Joel I.-J. Wang, Simon Gustavsson, and William D. Oliver. Superconducting qubits: Current state of play. *Annual Review of Condensed Matter Physics*, 11:369–395, 2020.
- [17] Arian Vezvaei, Vinay Tripathi, Daria Kowsari, Eli Levenson-Falk, and Daniel A. Lidar. Virtual-z gates and symmetric gate compilation. *PRX Quantum*, 6(2):020348, 2025.
- [18] Nello Cristianini, John Shawe-Taylor, Andre Elisseeff, and Jaz Kandola. On kernel-target alignment. In *Proceedings of the 15th International Conference on Neural Information Processing Systems: Natural and Synthetic*, NIPS’01, pages 367–373, Cambridge, MA, USA, January 2001. MIT Press.
- [19] Shunxin Wang, Raymond Veldhuis, Christoph Brune, and Nicola Strisciuglio. A survey on the robustness of computer vision models against common corruptions, 2024.
- [20] Dan Hendrycks and Thomas Dietterich. Benchmarking neural network robustness to common corruptions and perturbations, 2019.
- [21] Dimitris Achlioptas. Database-friendly random projections: Johnson-Lindenstrauss with binary coins. *Journal of Computer and System Sciences*, 66(4):671–687, June 2003.
- [22] Ping Li, Trevor J. Hastie, and Kenneth W. Church. Very sparse random projections. In *Proceedings of the 12th ACM SIGKDD international conference on Knowledge discovery and data mining*, KDD ’06, pages 287–296, New York, NY, USA, August 2006. Association for Computing Machinery.

- [23] Jonathon Shlens. A Tutorial on Principal Component Analysis, April 2014. arXiv:1404.1100 [cs].
- [24] Ian T. Jolliffe and Jorge Cadima. Principal component analysis: a review and recent developments. *Philosophical Transactions of the Royal Society A: Mathematical, Physical and Engineering Sciences*, 374(2065):20150202, April 2016.
- [25] Dong Yin, Raphael Gontijo Lopes, Jonathon Shlens, Ekin D. Cubuk, and Justin Gilmer. A fourier perspective on model robustness in computer vision. In *Advances in Neural Information Processing Systems 32 (NeurIPS 2019)*, pages 13276–13286. Curran Associates, Inc., 2019.
- [26] Kai Xu, Minghai Qin, Fei Sun, Yuhao Wang, Yen-Kuang Chen, and Fengbo Ren. Learning in the Frequency Domain, March 2020. arXiv:2002.12416 [cs].
- [27] José Augusto Stuchi, Levy Boccato, and Romis Attux. Frequency learning for image classification, June 2020. arXiv:2006.15476 [cs].
- [28] Matthew Tancik, Pratul P. Srinivasan, Ben Mildenhall, Sara Fridovich-Keil, Nithin Raghavan, Utkarsh Singhal, Ravi Ramamoorthi, Jonathan T. Barron, and Ren Ng. Fourier features let networks learn high frequency functions in low dimensional domains. In *Proceedings of the 34th International Conference on Neural Information Processing Systems, NIPS '20*, pages 7537–7547, Red Hook, NY, USA, December 2020. Curran Associates Inc.
- [29] Maria Schuld, Ryan Sweke, and Johannes Jakob Meyer. Effect of data encoding on the expressive power of variational quantum-machine-learning models. *Phys. Rev. A*, 103:032430, Mar 2021.
- [30] Jonas M. Kübler, Simon Buchholz, and Bernhard Schölkopf. The inductive bias of quantum kernels. In *Proceedings of the 35th International Conference on Neural Information Processing Systems, NIPS '21*, Red Hook, NY, USA, 2021. Curran Associates Inc.
- [31] Sau Lan Wu, Shaojun Sun, Wen Guan, Chen Zhou, Jay Chan, Chi Lung Cheng, Tuan Pham, Yan Qian, Alex Zeng Wang, Rui Zhang, Miron Livny, Jennifer Glick, Panagiotis Kl. Barkoutsos, Stefan Woerner, Ivano Tavernelli, Federico Carminati, Alberto Di Meglio, Andy C. Y. Li, Joseph Lykken, Panagiotis Spentzouris, Samuel Yen-Chi Chen, Shinjae Yoo, and Tzu-Chieh Wei. Application of quantum machine learning

using the quantum kernel algorithm on high energy physics analysis at the LHC. *Physical Review Research*, 3(3):033221, September 2021.

- [32] J. W. Cooley and John W. Tukey. An algorithm for the machine calculation of complex fourier series. *Mathematics of Computation*, 19(90):297–301, 1965. Introduces the FFT algorithm reducing DFT complexity from $O(N^2)$ to $O(N \log N)$ via divide-and-conquer recursion.
- [33] Ella Bingham and Heikki Mannila. Random projection in dimensionality reduction: Applications to image and text data. In *Proceedings of the Seventh ACM SIGKDD International Conference on Knowledge Discovery and Data Mining (KDD '01)*, pages 245–250. ACM, 2001. Shows that random projections are computationally simpler than PCA and effective for dimensionality reduction with low distortion.
- [34] Fan Yang, Sifan Liu, Edgar Dobriban, and David P. Woodruff. How to reduce dimension with pca and random projections? *arXiv preprint*, abs/2005.00511, 2020. Reviews differences between PCA (data-aware) and random projections (data-oblivious), noting speed advantages of random projections for dimensionality reduction.
- [35] Gabriele Agliardi, Giorgio Cortiana, Anton Dekusar, Kumar Ghosh, Naeimeh Mohseni, Corey O’Meara, Víctor Valls, Kavitha Yogaraj, and Sergiy Zhuk. Mitigating exponential concentration in covariant quantum kernels for subspace and real-world data. *npj Quantum Information*, 12:12, 2025.
- [36] James Lee-Thorp, Joshua Ainslie, Ilya Eckstein, and Santiago Ontañón. Fnet: Mixing tokens with fourier transforms. arXiv:2105.03824, 2021.
- [37] Marcos Alemany Manzanaro and Higinio Mora. Assessing the viability of quantum sat solvers: A comparative study using grover’s algorithm and quantum hardware. In Kohei Arai, editor, *Proceedings of the Future Technologies Conference (FTC) 2025, Volume 4*, pages 310–325, Cham, 2026. Springer Nature Switzerland.
- [38] Michael J. Bremner, Richard Jozsa, and Daniel J. Shepherd. Commuting quantum computations: post hoc distributed sampling and classical simulations. *Proceedings of the Royal Society A*, 467(2126):459–472, 2010.

- [39] Pablo Herrero-Gómez, Francisco Pujol-López, Ana Martínez García, and Higinio Mora Mora. Quantum computing models for financial analysis. In Hoai An Le Thi, Tao Pham Dinh, and Hoai Minh Le, editors, *Modelling, Computation and Optimization in Information Systems and Management Sciences*, pages 183–194, Cham, 2026. Springer Nature Switzerland.